Cell Reports
Physical Science

CellPress
OPEN ACCESS

Article

Accelerated design of vanadium redox flow battery electrolytes through tunable solvation chemistry

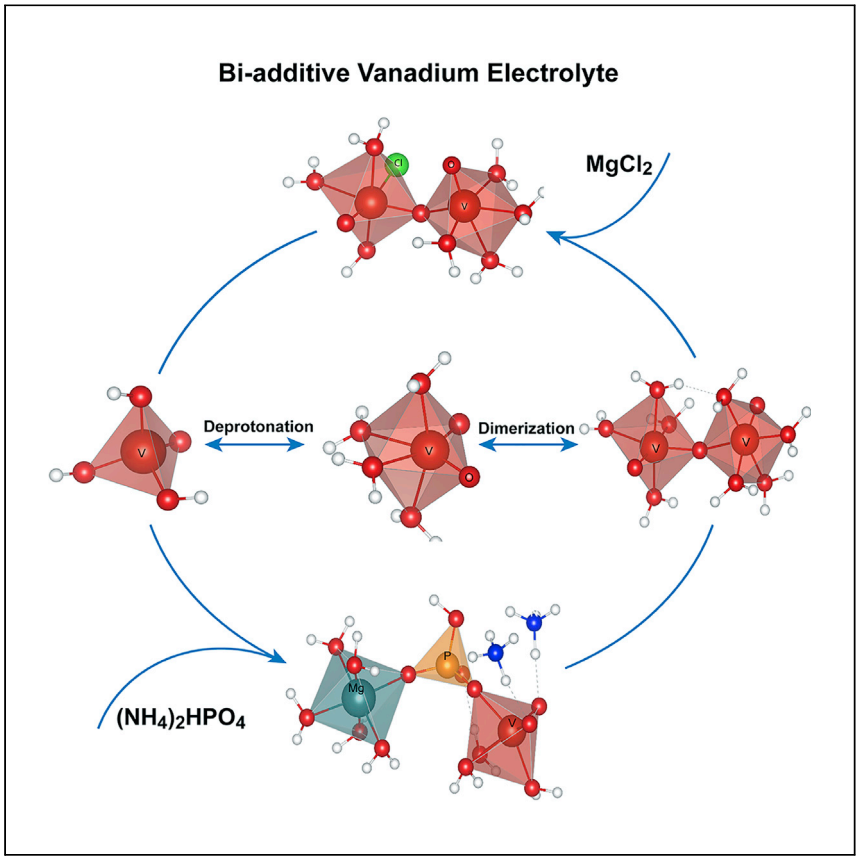

Murugesan et al. report a thermally stable vanadium redox flow battery electrolyte by tuning an aqueous solvation structure, exploiting competing cations and anions. This bi-additive-based electrolyte yields a more than 180% and more than 30% enhancement of thermal stability and energy density, respectively, relative to traditional sulfuric acid-based electrolytes.

Vijayakumar Murugesan, Zimin Nie, Xin Zhang, ..., Litao Yan, David Reed, Wei Wang

vijay@pnnl.gov (V.M.)
wei.wang@pnnl.gov (W.W.)

HIGHLIGHTS

Preferential interactions with additives render vanadium solvation structure tunable

Disruption of vanadium clustering process improves thermal stability of electrolyte

Mechanistic view of nucleation process using multimodal spectroscopic analysis

Bi-additive-based electrolyte nearly doubles the operational temperature window

Murugesan et al., Cell Reports Physical Science 2, 100323
February 24, 2021
https://doi.org/10.1016/j.xcrp.2021.100323

Cell Reports
Physical Science

CellPress
OPEN ACCESS

Article

Accelerated design of vanadium redox flow battery electrolytes through tunable solvation chemistry

Vijayakumar Murugesan,[1,*] Zimin Nie,[2] Xin Zhang,[1] Peiyuan Gao,[1] Zihua Zhu,[3] Qian Huang,[2] Litao Yan,[2] David Reed,[2] and Wei Wang[2,4,*]

SUMMARY

Operational stability of electrolytes is a persistent impediment in building redox flow battery technology. Stabilizing multiple vanadium oxidation states in aqueous solution is a primary challenge in designing reliable large-scale vanadium redox flow batteries (VRBs). Here we demonstrate that rationally selected ionic additives can stabilize the aqua vanadium solvate structures through preferential bonding and molecular interactions despite their relatively low concentrations ($\leq$0.1 M). The competing cations (NH_4^+ and Mg^{2+}) and bonding anions (SO_4^{2-}, PO_4^{3-}, and Cl^-) introduced by bi-additives are used to tune the vanadium solvation chemistry and design an optimal electrolyte for VRB technology. Such molecular engineering of VRB electrolytes results in enhancement of the operational temperature window by 180% and energy density by more than 30% relative to traditional electrolytes. This work demonstrates that tunable solvation chemistry is a promising pathway to engineer an optimal electrolyte for targeted electrochemical systems.

INTRODUCTION

Vanadium redox flow batteries (VRBs) have recently attracted research and development interest because of their high safety, long-term cycling, and capability to store and release a large amount of energy in a controlled manner, which are critical attributes of grid scale batteries.[1] Although multi-MWh (megawatt hour) scale-up installations have been demonstrated,[2] the current technology is still facing significant limitations in terms of solubility and thermal stability of catholyte ($V^{4+/5+}$) and anolyte ($V^{3+/2+}$) of the vanadium electrolyte solutions. Traditional sulfuric acid-based VRB electrolytes (catholyte and anolyte) often suffer from thermally induced precipitation as oxovanadium-based complexes.[3] In particular, the V_2O_5 precipitation from vanadium (V) catholyte solution at elevated temperature ($\geq$30°C) and higher concentrations ($\geq$1.5 M) has imposed serious limitations on practical applications of VRB technology. Recently, we demonstrated that thermal stability of the V cation relies on deprotonation of solvating water molecules.[4–6] The electron sharing between the high Lewis acidity V^{5+} center and oxygen of solvating water molecules causes a deprotonation process and initiates oxolation into multimeric oxovanadium structures (e.g., n(V—OH) → (V—O—V)$_n$ + nH$_2$O), which eventually leads to insoluble V_2O_5 powder precipitates. This not only explains the failure to inhibit precipitation by increasing the sulfuric acid concentration in early attempts[7–9] but offers a rationale to mitigate precipitation through introduction of competing anions that can engage electron sharing with V and potentially inhibit the deprotonation of water molecules.

[1]Physical and Computational Sciences Directorate, Pacific Northwest National Laboratory, Richland, WA 99354, USA

[2]Energy and Environmental Sciences Directorate, Pacific Northwest National Laboratory, Richland, WA 99354, USA

[3]Earth and Biological Sciences Directorate, Pacific Northwest National Laboratory, Richland, WA 99354, USA

[4]Lead contact

*Correspondence: vijay@pnnl.gov (V.M.), wei.wang@pnnl.gov (W.W.)

https://doi.org/10.1016/j.xcrp.2021.100323

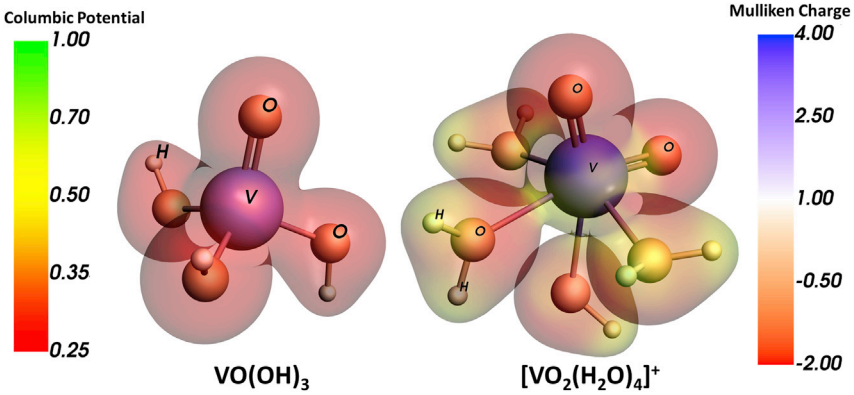

Scheme 1. Molecular view of deprotonated $VO(OH)_3$ species and parent $[VO_2(H_2O)_4]^+$ cation representing the V solvation structure in aqueous electrolyte

The solvation structures with the Coulombic potential map and Mulliken charge atomic coloring are derived from DFT-based calculations.

More recent development of mixed-acid V electrolytes (containing H_2SO_4 and HCl) significantly increased the concentration ($\geq$2 M) and high temperature stability ($\sim$50°C) of V^{5+} species.[10–12] In this system, the higher concentration of chloride anions (i.e., an $\sim$1:2 ratio of V:Cl) was used to establish viable contact-ion pair (CIP) formation with most of the V centers, which can ultimately suppress the deprotonation and subsequent precipitation process.[10,11] However, such high concentrations of chloride anions triggered preferential interactions with lower-order V species in the anolyte solution (in particular with V^{3+} cations), leading to a reversible gel-type precipitation process at lower temperatures (<0°C).[13] Oxovanadium-based precipitation in the catholyte and anolyte is generally initiated through a deprotonation process and populated through the oxolation process driven by molecular electrostatic potential. The electrostatic potential map of V molecular structures (Scheme 1) suggests that the negative surface potential is concentrated around V = O bonds and deprotonated water molecules that are prone to a dimerization process. We thus postulate that an effective additive molecule should not only have a CIP-compatible anion that can suppress deprotonation but should also contain competing ions that can disrupt multimeric cluster formation (dimer, trimer etc.).[14] For example, a cation that preferentially interacts with a dimerization site (i.e., V = O) and/or an anion serving as a bridging species between successive V centers can effectively disrupt degenerative oligomerization-type processes (e.g., –V–O–V–-type bond formation). However, identifying the optimal additive salt is non-trivial because it should have a higher dissociation constant and ions attuned to preferential interaction with all V center oxidation states. Here we report a bi-additive system consisting of di-ammonium hydrogen phosphate (DAP) and $MgCl_2$ salts that is formulated based on their preferential molecular and bonding interactions with V cations. This bi-additive electrolyte system increased the stable operational temperature window by 180% and the energy density by more than 30% relative to traditional sulfuric acid-based V electrolytes. We report the molecular-level preferential solvation structure of V molecules in the presence of bi-additive systems and the electrochemical performance of this newly designed flow battery electrolyte with enhanced thermal and chemical stability.

RESULTS

Additive formulation and testing

Based on our hypothesis (*vide supra*) that preferential molecular and bonding interactions of ionic species with V cations can enhance thermal stability, we explored

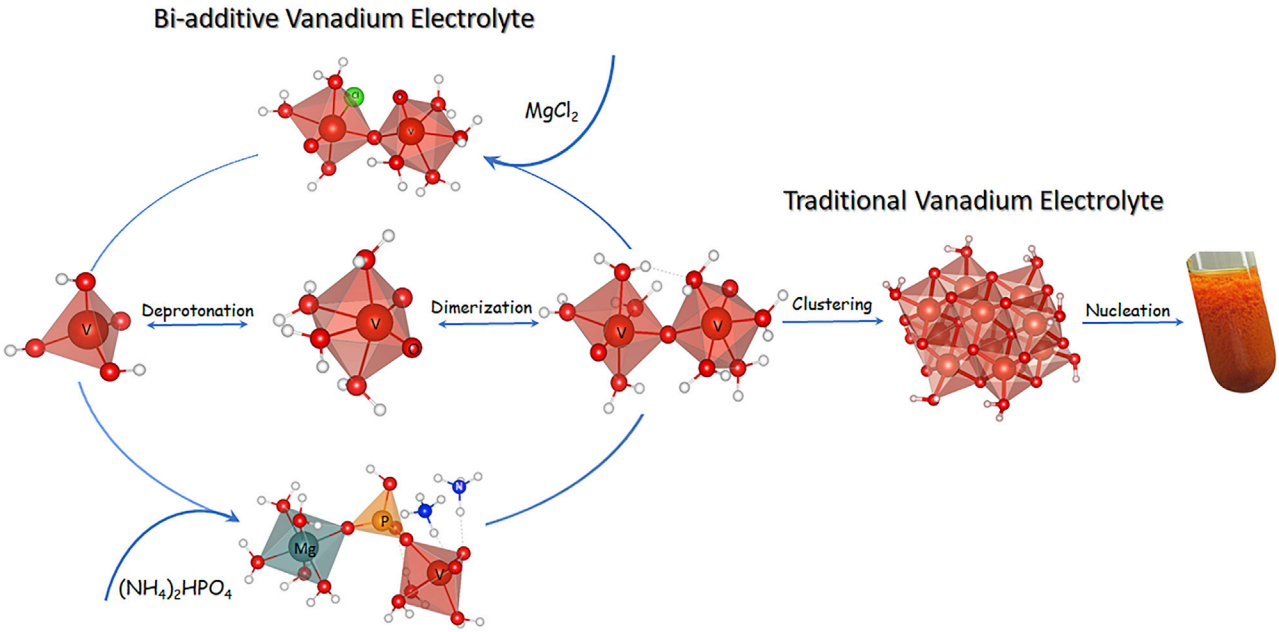

Scheme 2. Proposed V^{5+} cation molecular structural evolution and precipitation pathways for bi-additive and traditional electrolytes, respectively
The molecular process shown here are not based on *ab initio* energy calculations but hypothetical pathways based on multimodal spectroscopy analysis.

possible ionic salts as additive systems for VRB electrolytes. Typically, phosphate and chloride anion-based additives are preferred because they are known to establish CIP with all V cations (V^{n+} n = 2–5).[15–18] Literature analysis of various cation solvation phenomena reveals that magnesium (Mg^{2+}) and ammonium (NH_4^+) cations have a high dissociation rate with common counter anions, as evidenced by the very high solubility of the respective salts. Similarly, these cations can preferentially interact with the active V = O site, as evidenced by efficient intercalation of Mg^{2+} and NH_4^+ ions within V_2O_5 interlayers and from various ammonium- and magnesium-based vanadate crystalline structures.[19,20] Apart from the predicted dissociation and preferential interaction behaviors, the Mg^{2+} and NH_4^+ ions are also expected to preferentially interact with V structures and/or comprise part of the aqueous solvation structure (i.e., $[Mg.6H_2O]^{2+}$ and $[NH_4.xH_2O]^+$), where the highly labile nature of water molecules from the primary solvation sheath can ensure higher proton conductivity and lower viscosity of the redox flow battery electrolyte. Based on these rationales, we formulated a bi-additive system consisting of DAP (i.e., $(NH_4)_2HPO_4$) and $MgCl_2$ salts that could increase the V concentration and thermal stability window of the catholyte and anolyte of the VRB.

The traditional sulfuric acid-based electrolyte is prepared by dissolving 2 M $VOSO_4$ in 3.5 M H_2SO_4, (i.e., 2 M V^{n+}/5.5 M SO_4^{2-}; n = 2–5), which serves as the control electrolyte for testing our additive system. V electrolytes containing V^{3+} and V^{5+} are prepared electrochemically through a flow cell. The $MgCl_2$ and $(NH_4)_2HPO_4$ salts are subsequently added to the control electrolyte. To preserve the functional properties (such as viscosity and conductivity) of the traditional electrolyte, each additive content is limited to 10 atom % or less of the V concentration, with varying combinations between the two additives. Electrolytes with single additives were also prepared and tested for comparison. A static test was conducted first, in which traditional electrolytes and electrolytes with the additives at different oxidation states were prepared

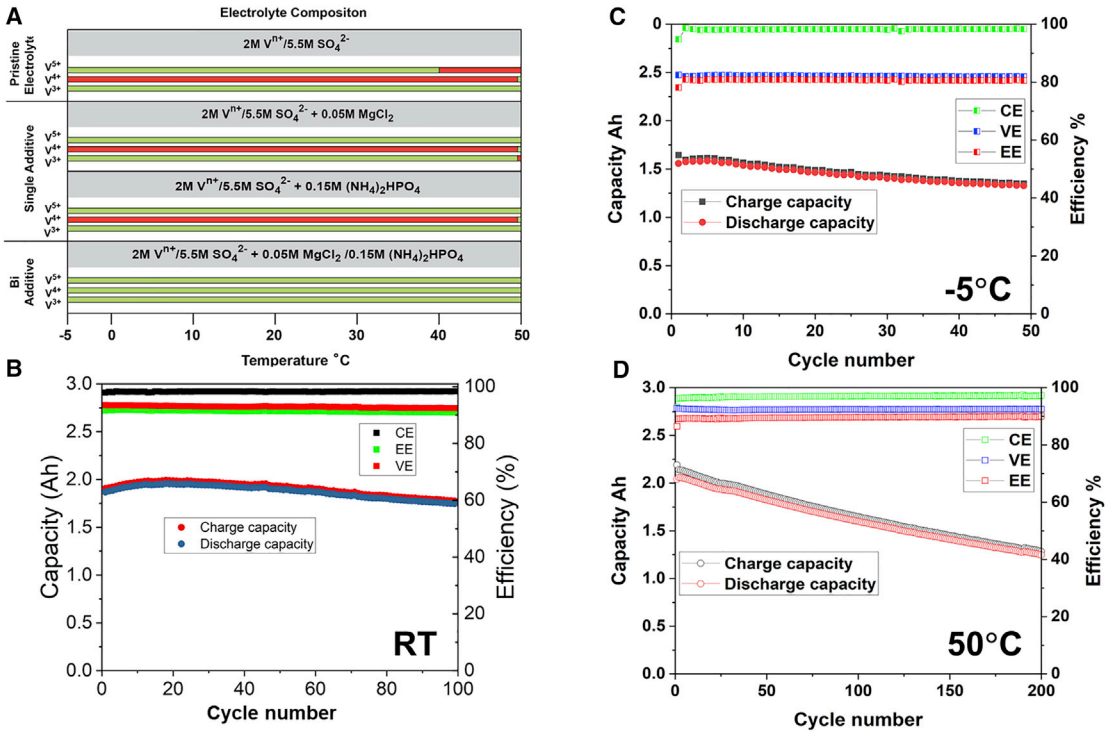

Figure 1. Testing the thermal stability of electrolytes and redox flow cell performance

(A) Static stability study of VRB electrolytes with selective additive molecules. The green and red lines represent stable and precipitated electrolyte solutions, respectively.

(B–D) Redox flow battery electrochemical test performance at different temperatures: (B) RT, (C) −5°C, and (D) 50°C.

electrochemically by charging the flow cell. These electrolytes were kept in environmental chambers at specific temperatures and examined periodically for precipitation. An electrolyte is deemed stable at a temperature when no precipitation is observed (visually) over a period of 10 days. The strong oxidizing ability of the V^{2+} cation prevented open air thermal stability analysis. Nevertheless, the thermal stability of the V^{2+} ion has not been reported as a major limiting factor in the VRB electrolyte.

Various concentrations and combinations of $MgCl_2$ and $(NH_4)_2HPO_4$ additives were studied. Detailed experimental data are summarized in Table S1. Figure 1A shows the stability study of a typical composition of additive-added electrolyte. As shown in Figure 1A, pristine 2 M V^{n+}/5.5M SO_4^{2-} electrolyte is not stable in a temperature range between −5°C to 50°C. In particular, the V^{5+} electrolyte has an upper temperature limit of 40°C, whereas the V^{4+} electrolyte has a lower temperature limit of 50°C, enforcing a V concentration limit of ~1.5 M for practical VRB applications. Even with this lowered V concentration, which resulted in reduced energy density, the VRB operational temperature window still needed to be restricted to 10°C–40°C to ensure a precipitation-free charge/discharge process. To enhance the thermal stability of electrolytes, the individual ionic additives $MgCl_2$ and $(NH_4)_2HPO_4$ were tested separately at 0.05 M and 0.15 M concentrations. Varying effects on electrolyte stability were found under these single-additive conditions (Figure 1A). The electrolyte with $MgCl_2$ extended the stability of V^{5+} while causing V^{3+} precipitation at 50°C. On the other hand, the $(NH_4)_2HPO_4$ salt enhanced V^{5+} stability but had no effect on the thermal stability of V^{4+} cations. However, the bi-additive system with $MgCl_2$ and $(NH_4)_2HPO_4$ significantly improved the stability of all V ions for catholyte

and anolyte electrolytes. Apparently, the synergistic effect of these two additives created a new V electrolyte that is stable at 2 M total V at a temperature range of −5°C to 50°C.

The bi-additive V electrolyte 2 M V^{n+}/5.5 M SO_4^{2-} + 0.05 M $MgCl_2$ + 0.15 M $(NH_4)_2HPO_4$ was then selected for the flow cell test. As shown in Figures 1B–1D, cycling tests of the bi-additive electrolyte were conducted in the environmental chamber at −5°C, room temperature (RT), and 50°C, respectively. At −5°C, the flow cell delivers Coulombic efficiency above 98% and energy efficiency of ~80% throughout 50 cycles with slight capacity decay, which is typical behavior for VRBs because of active material crossover through the membrane. The flow cell with the bi-additive electrolyte of the same composition demonstrated a much higher energy efficiency of ~89% because of reduced cell resistance at an elevated temperature of 50°C, whereas a lower Coulombic efficiency of ~97%, corresponding to a faster capacity decay rate over 200 cycles, was related to a more severe crossover effect. The cycling performance of the flow cell at 25°C falls between those tested at −5°C and 50°C in terms of efficiency and capacity decay. Throughout the cycling test of these three flow cells, no precipitation or other abnormal charge/discharge behavior was observed, which suggests that V^{2+} is also stable under this condition. Static electrolyte and dynamic flow cell tests have demonstrated significant improvement in thermal stability of the bi-additive electrolyte. A systematic study has been carried out to understand the solution chemistry and environment that contribute to the improved electrolyte stability. Because of the complexity of the bi-additive electrolyte system under different V oxidation conditions, in this study we only focus on the solvation phenomenon related to the high temperature stability of V^{5+} ions.

Multimodal spectroscopy analysis

The first step in analyzing the role of the additive material in thermal stability is to speciate the V clusters and their thermal evolution within the electrolyte solutions. We employed *in situ* liquid time-of-flight secondary-ion mass spectrometry (ToF-SIMS) to identify the nature of the clustered species (i.e., V-O-V-type structures) under various heat treatment conditions. Figure 2 shows the ToF-SIMS spectra of 2 M V electrolyte heat-treated at 50°C, clearly indicating the presence of various multimeric vanadate species with $V_nO_m^-$ ($n \leq 9$; $2 \geq m \leq 28$)-type structures in addition to monomeric $[VO_2]^+$ species. It should be noted that the observed structural diversity might be due to fragmentation of stable larger molecule(s) upon interaction with the higher kinetic energy of the primary Bi^{3+} ion beam, which is used to generate gas-phase ionic species from 2 M electrolyte solution. The detection of multimeric species (such as dimers, trimers, tetramers, etc.) for the traditional solution suggests the decavanadate species $[V_{10}O_{28}]^{6-}$ as the possible dominant species, even under RT conditions.[21] Formation of the decavanadate structure through hydrolysis and oligomerization processes under low pH (~2) and RT conditions has been reported previously.[22,23] Under prolonged heat treatment (50°C for 30 h) of the traditional electrolyte, the relative concentration of $V_nO_m^-$ clusters increases significantly, indicating thermally driven oligomerization of monomeric vanadate species. Conversely, the bi-additive electrolyte registers significantly lower concentrations of multimeric species relative to the traditional electrolyte, indicating suppression of the oligomerization process even after prolonged heat treatment (Figure 2B). Closer analysis reveals that unique species such as $[V_nO_m+HPO_4]^-$ and $[V_nO_m+MgO]^-$ were observed, suggesting that additive-based ionic species (PO_4^{2-} and Mg^{2+}) establish CIP formation with V solvates, which eventually suppressed the oligomerization-driven polyoxovanadate nucleation process. Although the fragmented

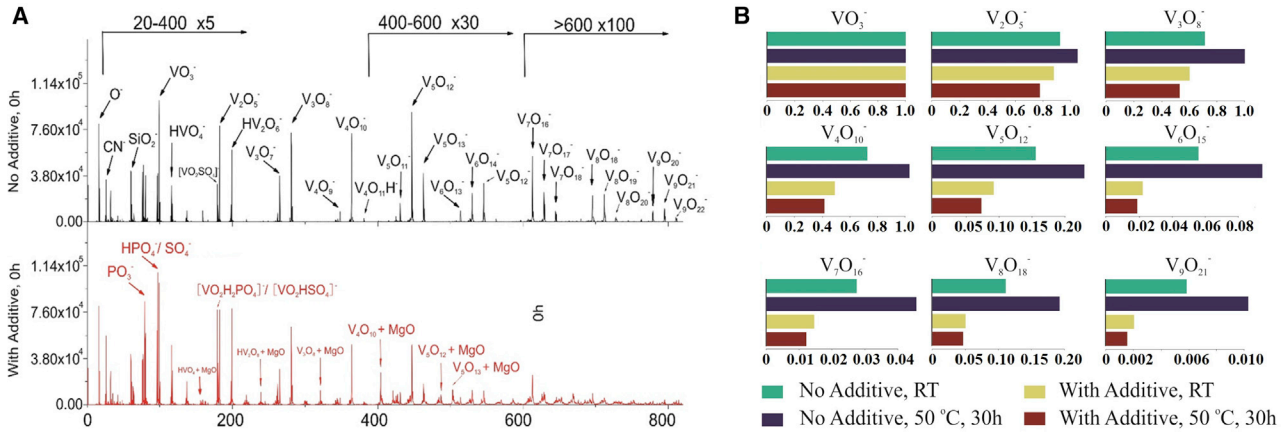

Figure 2. Probing V cluster formation using ToF-SIMS analysis

(A) SIMS spectrum of 2 M V^{5+} solution with (bottom) and without (top) additives before heat treatment.

(B) Compositional analysis of various V clusters in 2 M V^{5+} solution with/without additives before and after heat treatment at 50°C for 20 and 30 h based on *in situ* liquid cell ToF-SIMS analysis.

species detected in ToF-SIMS analysis is direct evidence of additive molecule association with vanadate species as well as the clustering process, their original molecular structures are still unclear. A molecular-level view of the bi-additive electrolyte system would require non-destructive spectroscopy analysis that is sensitive to molecular structure and associated dynamic processes. Hence, we performed Raman and nuclear magnetic resonance (NMR) spectroscopy measurements for the bi-additive electrolyte at elevated temperature to distinguish the V solvate structure and subsequent clustering process.

We began with the Raman analysis of the solvent system (5.5 M H_2SO_4), which yielded bands at 600 and 1,050 cm^{-1} representing SO_3 deformational and HSO_4^- asymmetrical stretches, respectively.[24,25] At 0.2 M V concentration, the traditional electrolyte system registers a new resonance around 935 cm^{-1}, representing monomeric aqua-vanadic ions (i.e., $[VO_2.3H_2O]^+$), which is known to be the dominant species at lower V concentrations.[24] At 2 M V concentration for the traditional and additive-based electrolytes, the intensity of this signature resonance drops, which coincides with emergence of a broad peak centered around 780 cm^{-1} representing the V-O-V stretch mode.[26,27] This clearly indicates evolution of multimeric vanadate as the dominant species in the 2 M electrolyte solution, in agreement with the ToF-SIMS measurements. Clustering of these multimeric V species through bridging oxygen could be the building block and, eventually, the nucleation centers for solid V_2O_5. Such precipitation processes can also be monitored by low-wave-number peaks (<300 cm^{-1}), which are signature resonances for solid-phase V_2O_5. For example, peaks at 139 and 160 cm^{-1} can represent the skeleton-bent vibration of V-O, and the 714 cm^{-1} peak would indicate the presence of a V-O-V bonding network of solid V_2O_5 structure.[26,27] To test this hypothesis of resonance peaks as a signature of multimeric species evolution to solid-phase V_2O_5, we performed *in situ* liquid cell Raman measurements at 70°C with increasing time, as shown in Figure 3.

We began with 2 M traditional electrolyte solutions to follow the clustering and nucleation process by tracking the signature V-O-V-resonant bands (Figure 1B). Evidently, under prolonged heating conditions, the band at low wave numbers (139 and 160 cm^{-1}), representing solid phase V-O-V, emerges as the dominant

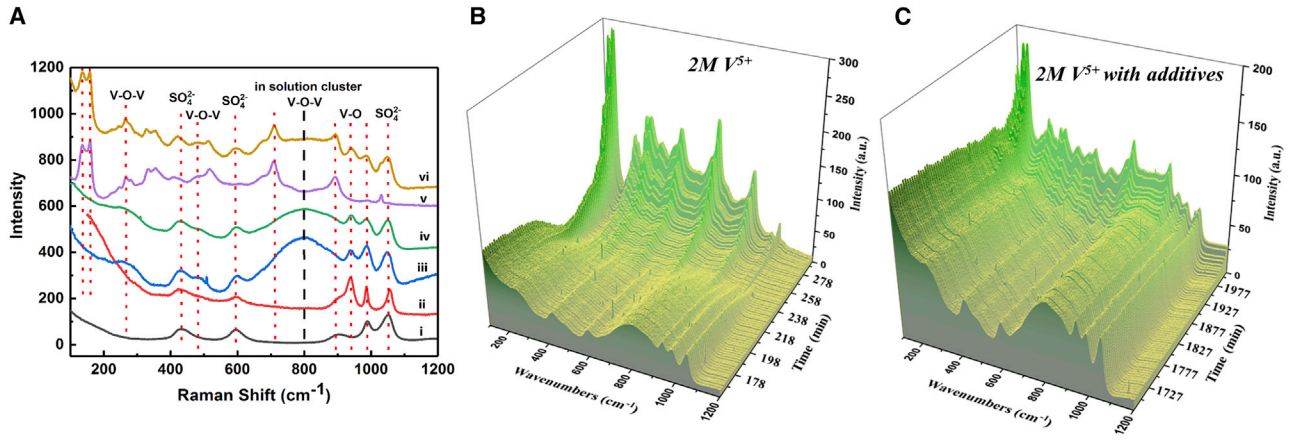

Figure 3. Probing the V_2O_5 nucleation mechanism using *in situ* Raman analysis

(A) Raman spectra of 5.5 M H_2SO_4 (i), 0.2 M V^{5+} (ii), 2 M V^{5+} (iii), 2 M V^{5+} with additives (iv), 2 M V^{5+} solution after heating at 70°C for 4.7 h (v), and 2 M V^{5+} solution with additives after heating at 70°C for 33.4 h (vi).

(B and C) *In situ* Raman spectra of 2 M V^{5+} solution without (B) or with additives (C) during heating at 70°C.

resonance at the expense of the broad resonance at 780 cm^{-1}, indicative of the molecular V-O-V stretch mode, which is part of multimeric vanadic species. These signature bands of solid-phase V_2O_5 become dominant after 204 min (3.4 h) and constant after 282 min, indicating near completion of the multimeric structure to V oxide evolution. Conversely, the 2 M bi-additive electrolyte shows emergence of solid-phase V_2O_5 resonances only after 1,832 min (30.5 h), which is about 10 times slower than the traditional electrolyte. It is clear that the *in situ* Raman analysis reveals that the native multimeric vanadic species evolve into solid-phase V_2O_5 at elevated temperatures and that the presence of additives significantly slows down the nucleation process. Nevertheless, understanding the role of additive species (i.e., phosphate, chloride, ammonium, and magnesium) in suppressing the nucleation process is still unclear. The low concentration ($\leq$0.1 M) of additive species in the electrolyte renders it difficult to probe using Raman spectroscopy, but nucleus-specific spectroscopy, such as NMR, is an effective tool to fill this gap.

Figure 4A shows ^{51}V NMR analysis of traditional and additive-based V electrolytes measured at 50°C under a 14-T magnetic field. The deconvoluted ^{51}V NMR spectra of the 2 M traditional electrolyte shows a broad peak at -569 ± 5 ppm ($\Delta_{1/2}$ ~17 kHz) along with a low-intensity peak at -535 ± 5 ppm ($\Delta_{1/2}$ ~8 kHz). The monomeric $[VO_2]^+$ cation is known to register a chemical shift around -530 ppm, which is in good agreement with the observed low-intensity peak.[5] Conversely, the high-intensity broad peak around -569 ± 5 ppm could represent multimeric vanadate structures such as the dimer (-569 ppm) and tetramer (-582 ppm) as well as the deprotonated $H_nVO_4^{n-3}$ anionic/neutral species (-560 ppm), as reported in the literature.[28–30] The peak ratio of these two components (10:90) reveals that the traditional electrolyte is dominated by multimeric structures at elevated temperatures. The 2 M bi-additive electrolyte registers three sharp ($\Delta_{1/2}$ < 1 kHz) and low-intensity peaks around -518, -539, and -583 ppm (with a total integral area of less than 10%) along with two broad peaks centered at -520 ± 5 ($\Delta_{1/2}$ ~30 kHz) and -610 ± 5 ppm ($\Delta_{1/2}$ ~20 kHz), representing the monomeric $[VO_2]^+$ cations and multimeric structures, respectively. The relative peak ratio of these broad components (60:40) infers suppression of the multimeric oxovanadium structure, as discussed for the ToF-SIMS and Raman analysis. Interestingly, the multimeric peak (approximately -610 ppm) is shifted toward a lower frequency relative to the traditional electrolyte, indicating

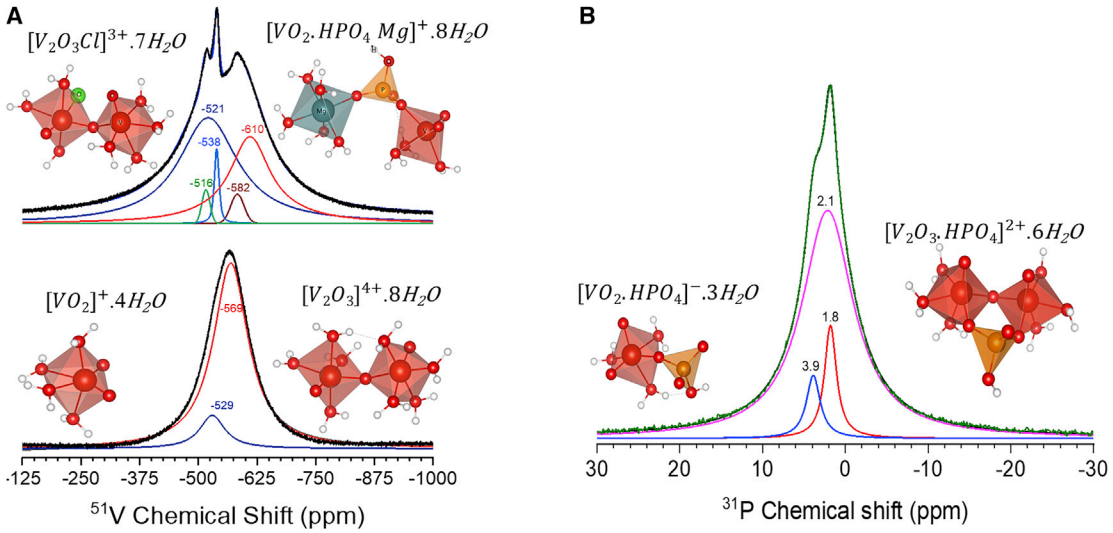

Figure 4. Role of additive molecules in V solvation structure using NMR

(A) ^{51}V NMR of traditional sulfuric acid (bottom) and bi-additive (top) based vanadium (V) electrolytes.

(B) ^{31}P NMR of bi-additive based V electrolyte. All the NMR spectra were collected using a liquids probe at 50°C under 14.1T magnetic field. The DFT-optimized molecular structures of probable oxovanadium species based on predicted NMR chemical shift are shown in the insert. The details of DFT calculations, predicted chemical shift and other relevant structural possibilities are shown in the supporting information.

possible coordination with counter anions (phosphate and chloride) and competing cations (NH_4^+ and Mg^{2+}). The CIP with chloride anions leading to the oxovanadium (V) chloride complex would register a chemical shift toward a higher frequency (less than −400 ppm).[4,12,31] However, there is no clear ^{51}V NMR resonance observed below −500 ppm, indicating that any chloride-based CIP formation could be a metastable structure prone to faster ligand exchange (less than milliseconds) with water molecules or induce broader line width (>100 kHz) beyond typical liquid NMR spectral resolution. Correspondingly, only PO_4^{2-} anions and Mg^{2+} cations are detected as CIP formation with the oxovanadium structure detected in our ToF-SIMS analysis (Figure 2). The CIP formation between Mg^{2+} cations and oxovanadium centers leading to V-O-Mg bonding is also evidenced as magnesium pyrovanadate ($Mg_2V_2O_7$) crystalline phases, which have ^{51}V chemical shift of about −603 ppm, in good agreement with the peak shifted to low frequency.[32] Similarly, CIP formation with PO_4 could cause a peak shift toward a lower frequency. For example, ion association with a PO_4 anion could lead to monomeric $[H_2PVO_7]^{2-}$, which reportedly has a ^{51}V chemical shift of −580 ppm, in agreement with the low-intensity sharp peak at −583 ppm for our bi-additive electrolytes.[17,33–35] Higher-order complexation with PO_4 anions could lead to dinuclear oxovanadium phosphate anions (i.e., $[H_4PV_2O_{10}]^-$) and even higher-order multimeric structures resembling the polymorphs of crystalline V phosphate structures, which are expected to produce larger chemical shifts in the range of −690 to −775 ppm.[36,37] It should be noted that the probable species discussed here are likely to be in equilibrium with their respective (de)protonated forms, which are likely to influence the observed chemical shift. The density functional theory (DFT)-predicted ^{51}V NMR chemical shifts of various oxovanadium molecules, along with experimental spectra of individual additive molecules, are reported (Figure S1). In addition, the possible clustering pathways based on chemical shift analysis are also discussed (Note S1; Figure S2).

The ^{31}P NMR spectrum of the bi-additive electrolyte reveals three unique phosphate species, with two sharp components around 1.8 and 3.9 ppm representing minority

species (<10%) and a broad component centered around 2.1 ppm. The minority species represented by two sharp lines matches the literature-reported ^{31}P chemical shifts of the phosphate anion of α-$VOPO_4$ and Keggin-type structure $[PV_{18}O_{46}]^{3+}$, respectively.[38] The unusually broad line width of the 4 ppm peak indicates suppressed rotational dynamics of the phosphate anion coordinated with the V cation (see supplemental information). For example, the dinuclear V species (di-μ-PO_4), such as $[H_4PV_2O_{10}]^-$, where the phosphate acts as a bridging species between successive V centers, will have suppressed rotational dynamics (Note S2; Figure S3). It is evident from the ^{31}P peak ratio that most of the phosphate anions are engaged in CIP formation, in particular with bridging-type coordination with V cations. This unique structural formation with the phosphate anion can disrupt the oxolation process and enhance the thermal stability of bi-additive electrolytes. Although CIP formation with the phosphate anion is evident, the roles of competing cations (i.e., NH^{4+} and Mg^{2+}) and prevalent SO_4^{2-} anions are unclear from the NMR analysis.

Ab initio computational analysis

To further probe the structural stability of additive-bonded vanadate molecules under a realistic electrolyte environment (with solvents and competing ions and solvent molecules) and thermal conditions, we employed *ab initio* molecular dynamics (AIMD) simulations. As a first step, we focused on CIP formation between counter anions (SO_4, PO_4, and Cl) and monomeric oxovanadium structure $[VO_2]^+$ (see supplemental information) to evaluate the thermodynamics of CIP formation. The interatomic distance between the V center and respective counter anion conditions remained constant during the time period of the simulation (20 ps), implying that CIP formation is thermodynamically viable even at elevated temperature (50°C). It should be noted that the AIMD-derived stability of CIP species (e.g., HSO_4-VO_2) could be limited to very short timescales (approximately picoseconds), whereas the typical ligand exchange process tends be relatively slower (microseconds or slower). Nevertheless, these CIP species could play a critical role in enhanced thermal stability through preferred interaction with adjacent oxovanadium centers. For example, the aqua $[VO_2]^+$ structure with CIP formation shows no evidence of the deprotonation process within the AIMD time window, even at 50°C. Hence, as a next step, we focused on the role of counter anions as bridging species that can disturb the long-range oxovanadium structure, such as extended $(V\text{-}O\text{-}V)_n$ bonding-type networks, which are known to be nucleation centers for V_2O_5 precipitation. We analyzed the dimeric oxovanadium species (i.e., [VO_2-μ-VO_2]), where the bridging species (μ) could be SO_4, PO_4, and Cl anions under realistic electrolyte conditions, such as with competing NH_4 cations in acidic solution. Even at the restricted timescale of AIMD, the dimeric species with SO_4 and Cl as bridging species were not thermodynamically favorable, as evidenced by bond breaking leading to a monomeric VO_2 and CIP species within 1 ps. Conversely, the phosphate anion establishes a stable dimeric species (i.e., [VO_2-HPO_4-VO_2]) in aqueous acidic solution, even under competing ions such as sulfate anions and ammonium cations. This preferential bonding of HPO_4^{2-} over SO_4^{2-} anions, even at very low concentrations (0.1 M versus 3.5 M), could be due to its relatively weaker interaction with solvent water molecules (see supplemental information). Such preferential bonding of HPO_4^{2-} anions as bridging species for V centers is also evidenced by the existence of diverse crystalline structures of $VOPO_4$. This also explains the criticality of lower phosphate concentrations in the additive system; higher concentrations could facilitate extended phosphate-bonded structural networks that would lead to $VOPO_4$ precipitation. As for the chloride anions, their interactions with oxovanadium species are likely to be restricted to CIP formation with faster ligand exchange processes, as evidenced by the absence of signature peaks in our spectroscopy analysis (*vide supra*).

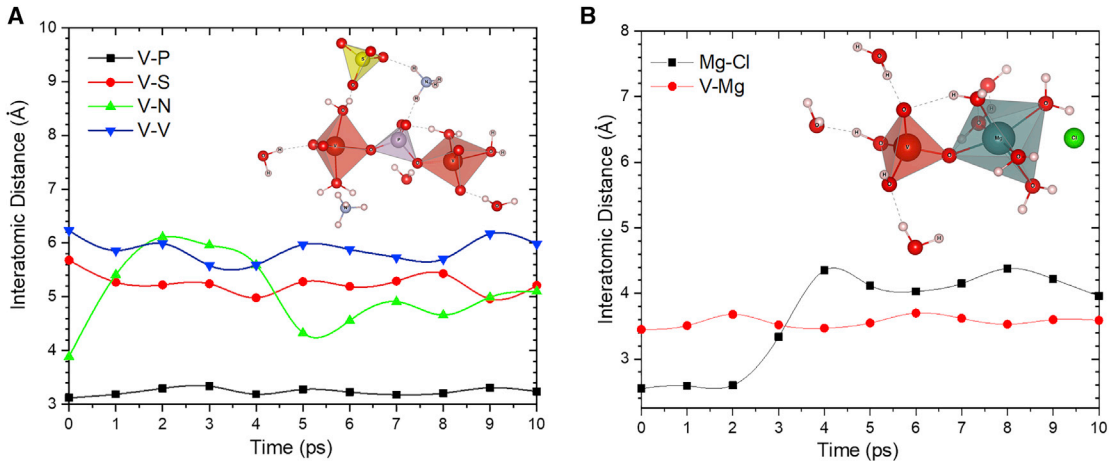

Figure 5. Evaluating thermodynamic stability of V clusters using AIMD simulation

(A) Time-dependent evolution of interatomic distances between the V core center and the $(NH_4)_2HPO_4$ additive molecule in sulfuric acid solution at 50°C. The inset molecular structure represents the dimeric V with phosphate as the bridging species at 10 ps.

(B) Time-dependent evolution of interatomic distances between the V core center and the $MgCl_2$ additive molecule in sulfuric acid solution at 50°C. The inset molecular structure represents the final V-O-Mg-based coordination complex molecule at 10 ps.

Despite their low concentrations and faster dynamics, chloride anion coordination with oxovanadium species could still serve as a suppressant of the deprotonation process and subsequent V_2O_5 nucleation process, as we reported earlier.[4,6]

Unlike the anions, the competing cations (i.e., NH_4^+ and Mg^{2+}) are not expected to establish CIP formation and suppress the deprotonation process but, rather, engage in coordination structure formation that can disrupt long range oxovanadium network-based nucleation centers. However, the weak coordination power of NH_4^+ with oxovanadium centers (e.g., V = O) prevents stable coordination complex formation in the solution. Based on AIMD analysis with phosphate anions as a bridging unit, NH_4^+ preferentially occupy the secondary solvation shell through electrostatic interaction with anion and oxygen centers (Figure 5A). On the other hand, Mg^{2+} is known to establish V-O-Mg bonding, which is the basis of magnesium vanadate-based polymorphic crystal structures. Evidently, the V-O-Mg-based coordination complex is detected in our ToF-SIMS analysis of bi-additive electrolyte solution (Figure 2B). To evaluate its molecular structure and associated thermodynamic stability, we performed an AIMD calculation with $[4H_2O.VO_2\text{-}Mg.6H_2O]^{+3}$ as the seed molecule and chloride and sulfate as counter anions. The result is shown in Figure 5B. At 50°C, the hydrated $[VO_2]^+$ structure undergoes immediate deprotonation, probably because of an enhanced positive atomic charge from the V-O-Mg-bonding character, leading to the $VO(OH)_3$ structure. This indicates that coordination with Mg is likely to enhance the oxolation-based clustering process because of a higher probability of hydroxyl groups within the oxovanadium structure. Various multimeric V structures with Mg coordination (such as V_4O_{10}+MgO, V_3O_8+MgO, and HV_2O_6+MgO) were detected in ToF-SIMS analysis, further validating the deprotonation-based clustering process hypothesized from the AIMD results. Nevertheless, these clustering processes based on V-O-Mg coordination complexes should be contained to avoid long-range network formation and subsequent metavanadate precipitation. The AIMD analysis revealed that the monomeric V-O-Mg-based coordination complex is thermodynamically stable, with chloride anions preferentially occupying the secondary solvation shell. The inherent nature of the Mg^{2+} cation, such as higher hydration enthalpy and surface

charge density, might impose a restriction on cluster size evolving from these coordination complexes. Mg^{2+} and phosphate anions clearly play a collective role in disrupting long-range network formation, whereas the chloride anion suppresses the deprotonation process through CIP formation. Based on our multimodal spectroscopy and computational elucidation of V solvation structural evolution, the underlying mechanism of the bi-additive electrolyte system is represented in a schematic in Figure 5. Nevertheless, we like to emphasize that a more detailed analysis is warranted to establish definitive molecular pathways and solvation structures within catholyte and anolyte solutions of the bi-additive electrolyte system.

DISCUSSION

We successfully demonstrated an additive development methodology for aqueous redox flow batteries based on tunable V solvation chemistry. Our methodology relies on the two-fold concept of (1) suppressing the deprotonation process through anion-based CIP formation and (2) disrupting the nucleation process through cation-based co-ordination complexes. We choose $MgCl_2$ and $(NH_4)_2HPO_4$ as additive materials that introduce competing cations and coordinating anions to alter the V solvation process and impede the nucleation process. These low-concentration ($\leq$ 0.1 M) additives increased the collective thermal stability of catholyte and anolyte and significantly increased the operational thermal window (−5°C to 50°C) and electrochemical performance of VRBs. The specific interactions of these additive molecules with the V solvation structure were analyzed using *in situ* multimodal spectroscopy techniques. The ToF-SIMS analysis and Raman spectroscopy provided direct evidence of additive roles in disrupting the V cation clustering process. The NMR chemical shift analysis combined with AIMD-based thermodynamic evaluation revealed the formation of unique co-ordination complexes and multimeric species with phosphate as bridging species. In particular, the spectroscopy signatures of the thermally induced V-O-V and V-O-Mg coordination complexes revealed their role in disrupting the initial nucleation process. Our approach shows that, by careful selection of cations and anions, the V solvation structure and emergent functionalities can be tuned for optimal redox flow battery electrolyte performance.

EXPERIMENTAL PROCEDURES

Resource availability

Lead contact

Further information and requests for resources and reagents should be directed to and will be fulfilled by the lead contact.

Materials availability

Materials synthesized in this manuscript can be obtained by request to the lead contact.

Data and code availability

This study did not generate code. All other experimental and computational data are available from the lead contact upon reasonable request.

Electrolyte materials and flow cell test

The V(IV) electrolyte solutions were prepared by dissolving $VOSO_4.xH_2O$ (Sigma-Aldrich, 97%) in H_2SO_4 (Sigma-Aldrich, 95.8%) acid solutions. The electrolyte solutions containing V(II), V(III), and V(V) cations were prepared electrochemically by charging the V(IV) solutions in a flow cell. For the stability study, a predetermined amount of additives was added to the electrolyte solutions before starting the stability tests. The stability tests were carried out at a temperature range of −5°C to 50°C in a

temperature-controlled environmental chamber (model BTL433, Espec North America). All stability tests were carried out statically (i.e., without any agitation). During the test, each sample was monitored twice a day for precipitation and solution color change.

A cyclic voltammogram (CV) was obtained with a potentiostat (Solartron 1287). Glassy carbon (CHI104, diameter 3 mm, CH Instruments, USA), a graphite counter electrode, and an Ag/AgCl reference electrode (CHI111, CH Instruments, USA) were employed in the CV test. The charge and discharge cyclic capability of the redox couple was evaluated with a flow cell designed in-house with a multichannel potentiostat (BT2000, Arbin Instruments, USA). The flow cell test setup includes one single cell, two electrolyte reservoirs, and two peristaltic pumps. A Nafion 115 membrane and a graphite felt electrode (GFD5, SGL Carbon, Germany) were employed in the single cell. Before the tests, the graphite felt was thermally oxidized in air at 400°C for 6 h to enhance electrochemical activity and hydrophilicity. The 2 M V/5 M H_2SO_4/0.05 M MgCl2/0.1 M $(NH_4)_2HPO_4$ electrolyte was selected for the flow cell tests. The electrolytes were circulated through the flow cell compartment by a peristaltic pump at a flow rate of 20 mL/min. Cyclic performance was evaluated by cycling between 1.2 and 1.6 V at 50 mA cm^{-2}. Cyclic tests were also carried out at different temperatures (−5 and 50°C) in an environmental chamber (model BTL433, Espec North America). The flow cell and two electrolyte reservoirs were located in the environmental chamber, but peristaltic pumps were outside of the chamber.

Spectroscopy measurements

The experimental parameters of vacuum-compatible *in situ* liquid SIMS measurement for molecular cluster analysis are discussed in the supplemental information and also in our previous publications.[39,40] A ToF-SIMS instrument (ION-TOF, Münster, Germany) was used in this research. The liquid cell was fabricated on a polyether ether ketone (PEEK) block on which a liquid chamber with a size of 3.0 mm (L) × 3.0 mm (W) × 0.3 mm (H) was machined with two liquid channels for introduction of electrolytes. A 100-nm-thick silicon nitride (SiN) membrane, which was attached at the bottom of a Si wafer (5.0 mm [L] × 5.0 mm [W] × 0.2 mm [H]), was immobilized (using epoxy glue) on top of the liquid chamber. An electrolyte could be introduced into the liquid chamber via the two liquid channels. After the ends of the two liquid channels were sealed, the liquid cell was loaded onto a ToF-SIMS sample holder for SIMS analysis. The vacuum pressure in the analysis chamber was 3×10^{-7} to 1.0×10^{-6} mbar during measurement. The primary ion beam was a pulsed (10 kHz) 25-keV Bi^{3+} beam focused on the SiN window with a spot size of ~450-nm diameter and an incident angle of 45° off the normal. The pulse width was about 150 ns, and the corresponding beam current was ~0.36 pA. For each measurement, the beam was scanned on a round area of ~2 μm in diameter on the SiN membrane to drill an aperture to expose liquid for analysis. After a mature aperture was formed, the Bi^{3+} pulse width was reduced from 150 ns to 50 ns (for better mass resolution) to collect a mass spectrum of the exposed electrolyte. A low-energy (~10-V) electron beam (flood gun) was used to compensate charging during analysis.

Raman spectra were recorded with a Horiba LabRam HR Evolution spectrometer coupled with an inverted optical microscope (Nikon Ti-E) with a 40× objective and a 632.8-nm HeNe laser light source. A quartz cell ($10 \times 10 \times 53$ mm^3) was used for the Raman measurements. The temperature of the liquid cell was controlled with an external temperature controller, and all Raman spectra were collected in the range of 150−4,000 cm^{-1}. The liquid state ^{31}P and ^{51}V NMR measurements were

performed using a Varian 600 Inova spectrometer (magnetic field B_0 = 14 T, where the ^{31}P and ^{51}V Larmor frequencies were 242.8 and 157.6 MHz, respectively), and their chemical shifts were referenced externally to a commercial 20% H_3PO_4 and clear $VOCl_3$ solution, respectively. NMR chemical shift calculations based on DFT were carried out using the ADF 2019 program.[41] The hybrid B3LYP function with Grimme dispersion correction (D3) and QZ4P (quad Z, 4 polarization functions, all electron) basis set was used for geometry optimization and chemical shift calculation. DFT calculations are carried out under a conductor-like screening model (COSMO) with water as a solvent.[41] It should be noted that DFT-based prediction of NMR chemical shifts is often marked by errors arising from the choice of parameters (such as functional, basis set, and continuum solvent model) and static molecular representation without solvation dynamics. Hence, the predicted NMR chemical shift can only be used as guidance rather than corroboration of the V speciation process.

Computational methods

AIMD simulations were carried out using the Vienna *ab initio* simulation package (VASP). Electron-ion interactions were described by the projector-augmented wave (PAW) pseudopotentials[42] with a cutoff energy of 500 eV. The exchange-correlation functional was represented using the revised Perdew-Burke-Ernzerhof generalized gradient approximation (GGA-revPBE).[43] The long-range van der Waals interaction was corrected by DFT-D3 with Becke-Jonson (BJ) damping method.[44] The exchange-correlation functional with a Gaussian smearing width term of 0.05 eV was used. The convergence criteria for electronic self-consistent iteration was set to 1×10^{-5} eV. Several VO_2^+-acid complex solution systems with additive salt were built for comparison. First, the VO_2^+-acid complexes were optimized by DFT calculation. Each system was solvated by randomly placing ~160 water molecules around the optimized structure. The system density was set to 1 g/cm^3. The thermodynamic stability of these VO_2^+-acid complexes in solution were investigated using AIMD simulations in the canonical ensemble at 50°C. The constant temperature of the AIMD simulation systems was controlled using a Nosé thermostat with a Nosé mass parameter of 0.1. A time step of 1 fs was used in all AIMD simulations. The product simulation time was 10–20 ps after energy minimization.

SUPPLEMENTAL INFORMATION

Supplemental Information can be found online at https://doi.org/10.1016/j.xcrp.2021.100323.

ACKNOWLEDGMENTS

The authors would like to acknowledge financial support primarily from the U.S. Department of Energy (DOE) Office of Electricity (OE) Energy Storage Program (under contract 57558). The NMR, Raman, and ToF-SIMS measurements and theoretical calculations were performed using EMSL (grid.436923.9), a DOE Office of Science User Facility sponsored by the Office of Biological and Environmental Research. PNNL is a multi-program national laboratory operated by Battelle for the DOE under contract DE-AC05-76RL01830.

AUTHOR CONTRIBUTIONS

Conceptualization, V.M. and W.W.; Methodology, V.M., Z.N., and W.W.; Investigation, X.Z., Z.N., L.Y., Q.H., and Z.Z.; Writing – Original Draft, V.M.; Writing – Review & Editing, W.W. and D.R.; Resources, L.Y., W.W., and Z.N.; Supervision, W.W., and D.R.

DECLARATION OF INTERESTS

The authors and their affiliated institute hold a United States patent (10673090 B2) related to findings reported in this article.

Received: October 19, 2020
Revised: December 7, 2020
Accepted: January 4, 2021
Published: January 25, 2021

REFERENCES

1. Wang, W., Luo, Q., Li, B., Wei, X., Li, L., and Yang, Z. (2013). Recent Progress in Redox Flow Battery Research and Development. Adv. Funct. Mater. *23*, 970–986.

2. Kamath, H., and Rajagopalan, S. (2007). Vanadium Redox Flow Batteries (Electric Power Research Institute).

3. Kazacos, M., Cheng, M., and Skyllas-Kazacos, M. (1990). Vanadium redox cell electrolyte optimization studies. J. Appl. Electrochem. *20*, 463–467.

4. Vijayakumar, M., Wang, W., Nie, Z., Sprenkle, V., and Hu, J. (2013). Elucidating the higher stability of vanadium(V) cations in mixed acid based redox flow battery electrolytes. J. Power Sources *241*, 173–177.

5. Vijayakumar, M., Li, L., Graff, G., Liu, J., Zhang, H., Yang, Z., and Hu, J.Z. (2011). Towards understanding the poor thermal stability of V5+ electrolyte solution in Vanadium Redox Flow Batteries. J. Power Sources *196*, 3669–3672.

6. Vijayakumar, M., Nie, Z., Walter, E., Hu, J., Liu, J., Sprenkle, V., and Wang, W. (2015). Understanding Aqueous Electrolyte Stability through Combined Computational and Magnetic Resonance Spectroscopy: A Case Study on Vanadium Redox Flow Battery Electrolytes. ChemPlusChem *80*, 428–437.

7. Cao, L., Skyllas-Kazacos, M., Menictas, C., and Noack, J. (2018). A review of electrolyte additives and impurities in vanadium redox flow batteries. J. Energy Chem. *27*, 1269–1291.

8. Kausar, N., Mousa, A., and Skyllas-Kazacos, M. (2016). The Effect of Additives on the High-Temperature Stability of the Vanadium Redox Flow Battery Positive Electrolytes. ChemElectroChem *3*, 276–282.

9. Skyllas-Kazacos, M., Peng, C., and Cheng, M. (1999). Evaluation of Precipitation Inhibitors for Supersaturated Vanadyl Electrolytes for the Vanadium Redox Battery. Electrochem. Solid-State Lett. *2*, 121–122.

10. Kim, S., Vijayakumar, M., Wang, W., Zhang, J., Chen, B., Nie, Z., Chen, F., Hu, J., Li, L., and Yang, Z. (2011). Chloride supporting electrolytes for all-vanadium redox flow batteries. Phys. Chem. Chem. Phys. *13*, 18186–18193.

11. Wu, X., Li, S., Huang, K., Ding, Z., Jiang, Z., Liu, S., and Li, X. (2011). Preparation, thermodynamic and electrochemical properties of vanadium solution. Acta Chimi. Sin. *69*, 1858–1864.

12. Li, L., Kim, S., Wang, W., Vijayakumar, M., Nie, Z., Chen, B., Zhang, J., Xia, G., Hu, J., Graff, G., et al. (2011). A Stable Vanadium Redox-Flow Battery with High Energy Density for Large-Scale Energy Storage. Adv. Energy Mater. *1*, 394–400.

13. Vijayakumar, M., Li, L., Nie, Z., Yang, Z., and Hu, J. (2012). Structure and stability of hexa-aqua V(III) cations in vanadium redox flow battery electrolytes. Phys. Chem. Chem. Phys. *14*, 10233–10242.

14. Penschke, C., Paier, J., and Sauer, J. (2018). Vanadium Oxide Oligomers and Ordered Monolayers Supported on CeO2(111): Structure and Stability Studied by Density Functional Theory. J. Phys. Chem. C *122*, 9101–9110.

15. Ouellette, W., Yu, M.H., O'Connor, C.J., and Zubieta, J. (2006). Structural diversity of the oxovanadium organodiphosphonate system: a platform for the design of void channels. Inorg. Chem. *45*, 3224–3239.

16. Beltrán-Porter, D., Amorós, P., Ibáñez, R., Martínez, E., Beltrán-Porter, A., Le Bail, A., Ferey, G., and Villeneuve, G. (1989). Synthetic pathways to vanadyl phosphates. Solid State Ion. *32*, 57–69.

17. Tietze, H. (1981). The crystal and molecular structure of oxovanadium(V) orthophosphate dihydrate, VOPO4.2H2O. Aust. J. Chem. *34*, 2035–2038.

18. Kato, R., Kobayashi, A., and Sasaki, Y. (1980). Heteropolyvanadate of phosphorus: preparation and structure. J. Am. Chem. Soc. *102*, 6571–6572.

19. Le, D.B., Passerini, S., Coustier, F., Guo, J., Soderstrom, T., Owens, B.B., and Smyrl, W.H. (1998). Intercalation of Polyvalent Cations into V_2O_5 Aerogels. Chem. Mater. *10*, 682–684.

20. Lee, S.H., Koo, J.M., Oh, S.G., and Im, S.S. (2017). Facile synthesis of ammonium vanadate nanofibers by using reflux in aqueous V_2O_5 solution with ammonium persulfate. Mater. Chem. Phys. *194*, 313–321.

21. Heath, E., and Howarth, O.W. (1981). Vanadium-51 and oxygen-17 nuclear magnetic resonance study of vanadate(V) equilibria and kinetics. J. Chem. Soc., Dalton Trans. *5*, 1105–1110.

22. Hayashi, Y. (2011). Hetero and lacunary polyoxovanadate chemistry: Synthesis, reactivity and structural aspects. Coord. Chem. Rev. *255*, 2270–2280.

23. Jin, K.P., Jiang, H.J., Wang, Y., Zhang, D.P., Mei, J., and Cui, S.H. (2018). Synthesis and Crystal Structure of Decavanadate-Based Coordination Polymers. J. Cluster Sci. *29*, 785–792.

24. Kausar, N., Howe, R., and Kyllas-Kazacos, M. (2001). Raman spectroscopy studies of concentrated vanadium redox battery positive electrolytes. J. Appl. Electrochem. *31*, 1327–1332.

25. Tomikawa, K., and Kanno, H. (1998). Raman study of sulfuric acid at low temperatures. J. Phys. Chem. A *102*, 6082–6088.

26. Baddour-Hadjean, R., Pereira-Ramos, J.P., Navone, C., and Smirnov, M. (2008). Raman microspectrometry study of electrochemical lithium intercalation into sputtered crystalline V_2O_5 thin films. Chem. Mater. *20*, 1916–1923.

27. Baddour-Hadjean, R., Smirnov, M.B., Smirnov, K.S., Kazimirov, V.Y., Gallardo-Amores, J.M., Amador, U., Arroyo-de Dompablo, M.E., and Pereira-Ramos, J.P. (2012). Lattice dynamics of β-V2O5: Raman spectroscopic insight into the atomistic structure of a high-pressure vanadium pentoxide polymorph. Inorg. Chem. *51*, 3194–3201.

28. Rehder, D., Polenova, T., and Bühl, M. (2007). Vanadium-51 NMR. In Annual Reports on NMR Spectroscopy, G.A. Webb, ed. (Academic Press), pp. 49–114.

29. Habayeb, M.A., and Hileman, O.E., Jr. (1980). 51V FT-NMR investigations of metavanadate ions in aqueous solutions. Can. J. Chem. *58*, 2255–2261.

30. McCann, N., Wagner, M., and Hasse, H. (2013). A thermodynamic model for vanadate in aqueous solution–equilibria and reaction enthalpies. Dalton Trans. *42*, 2622–2628.

31. Phan, V.M.T., Sharma, V., and Wuest, J.D. (1991). Multidentate Lewis acids. Adducts of monodentate and bidentate vanadyl dichloride alkoxides with ketones. Inorg. Chem. *30*, 3026–3032.

32. Nielsen, U.G., Jakobsen, H.J., and Skibsted, J. (2001). ^{51}V MAS NMR Investigation of ^{51}V Quadrupole Coupling and Chemical Shift Anisotropy in Divalent Metal Pyrovanadates. J. Phys. Chem. B *105*, 420–429.

33. Amoros, P., and Le Bail, A. (1992). Synthesis and crystal structure of α-NH4(VO2)(HPO4). J. Solid State Chem. *97*, 283–291.

34. Bircsak, Z., and Harrison, W.T.A. (1998). [alpha]-Ammonium Vanadium Hydrogen Phosphate, [alpha]-$(NH_4)V(HPO_4)_2$. Acta Crystallogr. C *54*, 1195–1197.

35. Fedotov, M.A., Maksimovskaya, R.I., and Kazanskii, L.P. (1981). Structure of vanadium phosphate anion in solutions from ^{17}O, ^{51}V and ^{31}P NMR data. React. Kinet. Catal. Lett. *16*, 185–189.

36. Frey, J., Sang Ooi, Y., Thomas, B., Reddy Marthala, V.R., Bressel, A., Schölkopf, T., Schleid, T., and Hunger, M. (2009). Vanadium phosphates on mesoporous supports: model catalysts for solid-state NMR studies of the selective oxidation of n-butane. Solid State Nucl. Magn. Reson. *35*, 130–137.

37. Siegel, R., Dupré, N., Quarton, M., and Hirschinger, J. (2004). ^{51}V magic angle spinning NMR in $VOPO_4$ phases. Magn. Reson. Chem. *42*, 1022–1026.

38. Shpeizer, B.G., Ouyang, X., Heising, J.M., and Clearfield, A. (2001). Synthesis and Crystal Structure of a New Vanadyl Phosphate $[H_{0.6}(VO)_3(PO_4)_3(H_2O)_3]\cdot 4H_2O$ and Its Conversion to Porous Products. Chem. Mater. *13*, 2288–2296.

39. Zhang, Y., Su, M., Yu, X., Zhou, Y., Wang, J., Cao, R., Xu, W., Wang, C., Baer, D.R., Borodin, O., et al. (2018). Investigation of Ion-Solvent Interactions in Nonaqueous Electrolytes Using in Situ Liquid SIMS. Anal. Chem. *90*, 3341–3348.

40. Zhang, Y., Zeng, W., Huang, L., Liu, W., Jia, E., Zhao, Y., Wang, F., and Zhu, Z. (2019). In Situ Liquid Secondary Ion Mass Spectrometry: A Surprisingly Soft Ionization Process for Investigation of Halide Ion Hydration. Anal. Chem. *91*, 7039–7046.

41. Velde, G.t., Bickelhaupt, F.M., Baerends, E.J., Guerra, C.F., Gisbergen, S.J.A.v., Snijders, J.G., and Ziegler, T. (2001). Chemistry with ADF. J. Comput. Chem. *22*, 931–967.

42. Kresse, G., and Joubert, D. (1999). From ultrasoft pseudopotentials to the projector augmented-wave method. Phys. Rev. B Condens. Matter Mater. Phys. *59*, 1758–1775.

43. Zhang, Y., and Yang, W. (1998). Comment on "Generalized Gradient Approximation Made Simple". Phys. Rev. Lett. *80*, 890.

44. Grimme, S., Ehrlich, S., and Goerigk, L. (2011). Effect of the damping function in dispersion corrected density functional theory. J. Comput. Chem. *32*, 1456–1465.